OXFORD

SOT | Society of Toxicology
www.toxsci.oxfordjournals.org

TOXICOLOGICAL SCIENCES, 152(2), 2016, 349–362

doi: 10.1093/toxsci/kfw093
Advance Access Publication Date: May 20, 2016
Research Article

Arsenite Uncouples Mitochondrial Respiration and Induces a Warburg-like Effect in *Caenorhabditis elegans*

Anthony L. Luz*, Tewodros R. Godebo*, Dhaval P. Bhatt†, Olga R. Ilkayeva†,‡, Laura L. Maurer*, Matthew D. Hirschey†,‡,§, and Joel N. Meyer*,[1]

*Nicholas School of the Environment, Duke University, Durham, North Carolina; †Duke Molecular Physiology Institute; ‡Sarah W. Stedman Nutrition and Metabolism Center; and §Departments of Medicine and Pharmacology & Cancer Biology, Duke University School of Medicine, Durham, North Carolina

[1]To whom correspondence should be addressed. Fax: 919-668-1799. E-mail: joel.meyer@duke.edu.

ABSTRACT

Millions of people worldwide are chronically exposed to arsenic through contaminated drinking water. Despite decades of research studying the carcinogenic potential of arsenic, the mechanisms by which arsenic causes cancer and other diseases remain poorly understood. Mitochondria appear to be an important target of arsenic toxicity. The trivalent arsenical, arsenite, can induce mitochondrial reactive oxygen species production, inhibit enzymes involved in energy metabolism, and induce aerobic glycolysis *in vitro*, suggesting that metabolic dysfunction may be important in arsenic-induced disease. Here, using the model organism *Caenorhabditis elegans* and a novel metabolic inhibition assay, we report an *in vivo* induction of aerobic glycolysis following arsenite exposure. Furthermore, arsenite exposure induced severe mitochondrial dysfunction, including altered pyruvate metabolism; reduced steady-state ATP levels, ATP-linked respiration and spare respiratory capacity; and increased proton leak. We also found evidence that induction of autophagy is an important protective response to arsenite exposure. Because these results demonstrate that mitochondria are an important *in vivo* target of arsenite toxicity, we hypothesized that deficiencies in mitochondrial electron transport chain genes, which cause mitochondrial disease in humans, would sensitize nematodes to arsenite. In agreement with this, nematodes deficient in electron transport chain complexes I, II, and III, but not ATP synthase, were sensitive to arsenite exposure, thus identifying a novel class of gene-environment interactions that warrant further investigation in the human populace.

Key words: arsenite; Warburg effect; *Caenorhabditis elegans*; mitochondrial toxicity.

INTRODUCTION

Over 140 million people worldwide consume arsenic contaminated drinking water that exceeds the World Health Organization's limit of 10 ppb (Ravenscroft *et al.*, 2009), with some of the highest concentrations of arsenic occurring in ground water in Bangladesh and West Bengal (Rahman, 2002). In this region of the world 35–77 million people are exposed to drinking water arsenic concentrations that range from less than 10 ppb to over 4 ppm, and as many as 1 in 5 deaths are attributed to arsenic exposure (Argos *et al.*, 2010; Rahman, 2002). Although the United States complies with the WHO's maximum contaminant level for municipal water supplies, private wells are rarely monitored, leaving millions of individuals at risk for chronic arsenic exposure. Lower levels of arsenic exposure may also be problematic. In New Hampshire, where 40% of residents own private wells, 10% of which exceed the 10 ppb limit (Karagas *et al.*, 2002), exposure has been associated with the development of squamous cell carcinomas (Gilbert-Diamond *et al.*, 2013) and bladder cancer (Karagas *et al.*, 2004), suggesting that private wells need to be monitored or that the current contaminant limit is not stringent enough.

In addition to skin (Yu *et al.*, 2006) and bladder (Marshall *et al.*, 2007) cancer, arsenic is also associated with kidney (Yuan *et al.*, 2010), liver (Liaw *et al.*, 2008), and lung (Smith *et al.*, 2006) cancer, and has been implicated in metabolic syndrome (Ditzel *et al.*, 2015; Shi *et al.*, 2013), and other metabolism-related

pathologies (Arteel *et al.*, 2008; Sanchez-Soria *et al.*, 2014; Tan *et al.*, 2011). However, despite decades of research, arsenic's precise mechanism(s) of inducing disease remains poorly understood. Reactive oxygen species (ROS) production (Shi *et al.*, 2004), DNA damage (Wang *et al.*, 2001), altered DNA methylation (Zhao *et al.*, 1997), and enzyme inhibition (Kitchin and Wallace, 2008) are all thought to play a role. Growing evidence indicates that mitochondria are an important cellular target of arsenic toxicity. Arsenite can enter mitochondria via aquaglyceroporins, where it can bind and inhibit numerous enzymes involved in energy production, including pyruvate, succinate, isocitrate, and α-ketoglutarate dehydrogenases (Bergquist *et al.*, 2009; HigashiI *et al.*, 1965; Hosseini *et al.*, 2013), as well as complexes II and IV of the electron transport chain (ETC) (Naranmandura *et al.*, 2011), suggesting arsenic-induced mitochondrial dysfunction may play a role in arsenic-related pathologies.

Interestingly, chronic, low-dose (75 ppb) arsenite exposure was recently shown to induce the Warburg effect, which is defined as a shift from mitochondrial oxidative phosphorylation (OXPHOS) to aerobic glycolysis and is a hallmark in the development of many cancers, in several pulmonary epithelial cell lines (Zhao *et al.*, 2013). Importantly, the observed glycolytic shift was accompanied by reduced Krebs cycle activity, increased aneuploidy, and a loss of anchorage dependent growth, all of which were dependent upon stabilization of the transcription factor, hypoxia inducible factor-1 alpha (HIF-1A) (Zhao *et al.*, 2014), further implicating disruption of mitochondrial energy metabolism as an important mechanism in arsenic carcinogenesis. The potential for environmental exposures to contribute to carcinogenesis via altered mitochondrial metabolism has recently been reviewed, but there are as yet few examples of such a mechanism (Robey *et al.*, 2015).

However, the aforementioned studies were performed *in vitro*, and because mitochondrial function is highly dependent upon cellular context and intercellular signals (McBride *et al.*, 2006), many of which are lost *in vitro*, it is important to test these results *in vivo*. The model organism *Caenorhabditis elegans* represents an excellent *in vivo* model for studying arsenic-induced mitochondrial dysfunction, as mitochondrial biology (Tsang and Lemire, 2003) and core metabolic pathways (Braeckman *et al.*, 2009) are well conserved with humans. Furthermore, transgenic strains such as the PE255 ATP reporter strain (Lagido *et al.*, 2008), as well as strains with mutations in mitochondrial genes can be used to rapidly assess the *in vivo* mitochondrial effects of arsenic. Here, utilizing *C. elegans*, we demonstrate an *in vivo* induction of glycolysis, which is accompanied by severe mitochondrial dysfunction (altered pyruvate metabolism, increased proton leak, and reduced ATP, ATP-linked respiration, and spare respiratory capacity) following exposure to arsenite. Our results both confirm *in vivo* outcomes observed previously *in vitro*, and demonstrate novel mitochondrial outcomes, further expanding our knowledge of the mechanisms underlying arsenite-induced metabolic dysfunction.

MATERIALS AND METHODS

C. elegans strains and culture conditions. Age-synchronized populations of L1 (larval stage 1) nematodes were obtained via sodium hydroxide bleach treatment as previously described (Boyd *et al.*, 2009), followed by an overnight incubation in complete K-medium (150 µl 1 M $CaCl_2$, 150 µl 1 M $MgSO_4$, 25 µl 10 mg/ml cholesterol, 50 ml sterile K-medium (2.35 g KCl, 3 g NaCl, 1 l ddH_2O)) on an orbital shaker at 20 °C. Synchronized *C. elegans* were then cultured on K-agar plates seeded with *Escherichia coli* OP50 as previously described (Lewis and Fleming, 1995; Stiernagle, 1999), whereas arsenite exposed nematodes were fed UVC-inactivated *E. coli* (UvrA-deficient strain, which lacks nucleotide excision repair and thus cannot repair UVC-induced DNA damage). Inactivated UvrA was generated via exposure to 1000 J/m^2 UVC using an ultra violet lamp (UVLMS-38 EL Series 3UV Lamp, UVP, Upland, California) with peak emission at 254 nm as described (Meyer *et al.*, 2010).

Wild type (N2 Bristol), ETC complex I (MQ1333 *nuo-6* (*qm200*; outcrossed × 6)), complex II (TK22 *mev-1* (*kn1*; outcrossed × 5)), complex III (MQ887 *isp-1* (*qm150*; outcrossed × 3), MQ989 *isp-1*(*qm150;* outcrossed × 3)*; ctb-1* (*qm189*)), complex V (LB127 *atp-2* (*ua2*; outcrossed × 6)), pyruvate kinase (VC1265 *pyk-1* (*ok1754*; outcrossed × 0)), lactate dehydrogenase (VC1767 *ldh-1* (*gk3142*; outcrossed × 0)), uncoupling protein 4 (CY121 *ucp-4* (*ok195*; outcrossed × 5)), beclin-1 (VC517 *bec-1* (*ok691*; outcrossed × 1)), VC893 *atg-18* (*gk378*; outcrossed × 1), hypoxia inducible factor-1 (ZG31 *hif-1a* (*ia4*; outcrossed × 9), ZG596 *hif-1a* (*ia7*; outcrossed × 4)), and superoxide dismutase (*sod-2* (*gk257*); *sod-3* (*tm760*), *sod-1* (*tm776*); *sod-4* (*gk101*); *sod-5* (*tm1146*)) mutants were obtained from the *Caenorhabditis* Genetics Center (CGC, University of Minnesota), and maintained at 20 °C. The germline-deficient strain JK1107 *glp-1* (*q224*; outcrossed > 1) was also purchased from the CGC, whereas the transgenic, luciferase-expressing PE255 *glp-4* (*bn2*) strain was generously provided by Dr. Christina Lagido, University of Aberdeen (Aberdeen, UK). Germline deficient strains were maintained at the permissive temperature of 15 °C until the time of the experiment when they were shifted to the restrictive temperature of 25 °C. All nematode strains will henceforth be referred to by their gene name.

Arsenite exposure. For all experiments, approximately 5000 young adult (raised on OP50 seeded K-agar at 25 °C for 48h) PE255 *glp-4* or *glp-1* nematodes were exposed to 0, 50, 250, or 500 µM sodium arsenite (Ricca Chemical Company, dissolved in ddH_2O) in complete K-medium containing UVC-killed UvrA (killed UvrA was added in a 1:5 ratio of bacterial culture resuspended in complete K medium to exposure medium) for 12, 24, or 48 h (12 and 24 h exposures were only performed for metabolomics analysis) with shaking at 25 °C. Following all arsenite exposures, nematodes were rinsed 4 times with K-medium to remove excess bacteria and arsenite, and then placed on an orbital shaker for 20 min at 25 °C to allow bacteria to clear from the nematode gut. Nematodes were then rinsed a final time with unbuffered reconstituted moderately hard water (EPA H_2O, 60 mg $MgSO_4{\cdot}7H_2O$, 60 mg $CaSO_4{\cdot}2H_2O$, 4 mg KCl per 1 l ddH_2O) (Weber, 1991) prior to assessing the mitochondrial endpoints outlined below.

Metabolic inhibition assay. To rapidly assess the effects of arsenite on mitochondrial function, we developed a novel assay that permits *in vivo* assessment of the relative degree of chemical-induced inhibition of different metabolic processes that contribute to maintenance of ATP levels (Luz *et al.*, 2016). Changes in ATP levels following short-term incubation with well-known inhibitors of mitochondrial energy metabolism (optimized conditions presented in Table 1) were measured in arsenite-exposed nematodes. Following 48 h of arsenite exposure, nematodes were resuspended in unbuffered EPA water to a final concentration of 1.0 ± 0.2 nematodes/µl. Approximately 50 nematodes per sample were pipetted into white 96-well plates using pipette tips rinsed in 0.1% Triton X-100 to prevent worm loss due to sticking. Four technical replicates (ie, 4 wells) of each

treatment were run per experiment. Inhibitors (listed in Table 1) were added to achieve a 1× final concentration, and the remaining volume was adjusted to 100 μl with unbuffered EPA water. Appropriate EPA water, DMSO controls, and 4 blank (unbuffered EPA H_2O) wells were included in each 96-well plate.

Following inhibitor exposure, as outlined in Table 1, steady state ATP levels were measured as previously described (Lagido *et al.*, 2008, 2015). Briefly, GFP fluorescence was measured (emissions filter: 502 nm; excitation filter: 485 nm) using a FLUOstar Optima plate reader (BMG Labtech, Offenburg, Germany). Luminescence buffer (140 mM Na_2PO_4, 30 mM citric acid (pH 6.5), 1% DMSO, 0.05% Triton X-100, 100 μM D-luciferin) was injected into each well and luminescence was measured 3 min later using a luminescence optic (BMG Labtech). Luminescence values were then normalized to GFP expression. The average effect of each inhibitor on ATP levels in arsenite exposed nematodes was then normalized to either the EPA water or DMSO control within each treatment group, and expressed as percent change of control. All experiments were repeated at least 3 separate times.

Metabolomics analysis. Nematodes (*glp-1*) were exposed to arsenite for 12, 24 or 48 h as outlined above, and then frozen for metabolomics analysis. Briefly, *C. elegans* samples were rinsed once with ice cold PBS, resuspended in 300 μl ddH_2O containing 0.6% formic acid, flash frozen in liquid nitrogen, and then stored at -80 °C until metabolite extraction.

To extract metabolites, all samples were thawed on ice and then sonicated on ice, using five 30 s on-off pulses at 20% power (Biologics, Inc., Virginia). An aliquot was saved for total protein analysis via bicinchonic acid assay (Thermo Fisher Scientific, Rockford, Illinois). Remaining sample was mixed with acetonitrile (1:1 ratio), vortexed, and divided in a 1:3 ratio for amino acid and acyl carnitine, and organic acid quantification. Amino acids and acylcarnitines were analyzed using MS/MS as previously described (An *et al.*, 2004; Wu *et al.*, 2004) and organic acids were quantified using GC/MS as described in (Jensen *et al.*, 2006). Raw data were normalized to protein, and then converted to $\log_2$ fold change relative to untreated nematodes.

Seahorse analysis. Using a Seahorse XF^e24 Bioanalyzer (Seahorse Bioscience, Massachusetts), we measured the fundamental parameters of the mitochondrial respiratory chain: basal oxygen consumption rate (OCR), ATP-linked respiration, maximal OCR, spare respiratory capacity (SRC), and proton leak, as previously described (Luz *et al.*, 2015a,b). Briefly, nematodes were suspended in unbuffered EPA water to a final concentration of 1.0 ± 0.2 nematodes/μl. 50 nematodes were then pipetted into each well of a 24-well utility plate (6 or 7 wells for each treatment, leaving 2 wells as blanks), and the final well volume was brought to 525 μl with unbuffered EPA water. An aliquot of nematodes was then collected and stored at -80 °C for total protein determination. Following an initial 8 basal OCR measurements, nematodes were exposed to either 25 μM FCCP (mitochondrial uncoupler), 20 μM DCCD (ATP synthase inhibitor) or 10 mM sodium azide (cytochrome *c* oxidase inhibitor), followed by an additional 8, 14, or 4 OCR measurements, respectively, for each inhibitor. SRC was calculated by subtracting a well's average basal OCR from its FCCP-induced maximal OCR. ATP-linked respiration was calculated by subtracting a well's DCCD response from its basal OCR, whereas proton leak was calculated by subtracting a well's response to sodium azide from the well's response to DCCD. OCR measurements were normalized to total protein.

Steady state ATP levels. Steady state ATP levels were measured in *glp-1* nematodes as previously described (Brys *et al.*, 2010). Briefly, nematodes were flash frozen in K-medium and stored at -80 °C until time of analysis. On the day of analysis, 10% trichloroacetic acid was added to each frozen sample, and samples were allowed to thaw on ice. 0.5 mm Zirconia beads were then added to each sample, and samples were then homogenized using a bullet blender (Next Advance, Averill Park, NY), run at maximum speed for three 45 s pulses at 4 °C. Samples were then neutralized via the addition of 1.33 mM $KHCO_3$ and Sigma water (St. Louis, Missouri). Aliquots of each sample were then saved on ice for total protein determination. The remainder of each sample was then transferred to a new micro-centrifuge tube, vacuum centrifuged at 4 °C for 10 min to remove air bubbles, and finally centrifuged at 14,000 rpm for 8 min at 4 °C to pellet protein. Samples were then diluted 1:10 and 1:50 in Sigma water for ATP determination via the Molecular Probes ATP Determination Kit (Invitrogen/Life Technologies, Carlsbad, CA). Luminescence was measured using a FLUOstar Optima plate reader equipped with a luminescence optic. Calculated ATP concentrations were normalized to total protein.

Mitochondrial and nuclear DNA copy number determination. Mitochondrial (mtDNA) and nuclear (nucDNA) DNA copy number were determined as previously described (Rooney *et al.*, 2015). Briefly, 6 nematodes were added to lysis buffer containing proteinase K using a platinum worm pick, and frozen at -80 °C. Thawed samples were then lysed via a 1 h incubation at 65 °C. Crude worm lysate was then used as template DNA for real-

TABLE 1. Preparation of Inhibitors for Metabolic Inhibition Assay

Inhibitor	Inhibitor target	Incubation length (h)[a]	8× working stock (%DMSO)	Final concentration (%DMSO)
2% DMSO	Control	1	16%	2%
Sodium azide	ETC Complex IV	1	80 mM (100% EPA H_2O)	10 mM (100% EPA H_2O)
FCCP	Mitochondrial Uncoupler	1	200 μM (16%)	25 μM (2%)
1% DMSO	Control	3	8%	1%
Rotenone	ETC Complex I	3	80 μM (8%)	10 μM (1%)
TTFA	ETC Complex II	3	8 mM (8%)	1 mM (1%)
Antimycin A	ETC Complex III	3	80 μM (8%)	10 μM (1%)
DCCD	ATP Synthase	3	160 μM (8%)	20 μM (1%)
DCA	Pyruvate Dehydrogenase Kinase	4.5	8 mM (100% EPA H_2O)	1 mM (100% EPA H_2O)
2-DG	Glycolysis	4.5	400 mM (100% EPA H_2O)	50 mM (100% EPA H_2O)

[a]Inhibitor incubation periods were chosen based on Seahorse XF^e Bioanalyzer experiments, whereas a 4.5 h incubation was chosen for 2-DG as this incubation period resulted in the greatest depletion of ATP in the context of arsenite exposure (data not shown).

time PCR determination of copy number. Standard curves were used for absolute determination of mtDNA and nucDNA copy number. Three samples of each treatment were collected per experiment. Each experiment was repeated 3 separate times.

Isolation of mitochondria for ICP-MS analysis. Following arsenite exposure, nematodes were rinsed 2 times with ice cold MSM buffer (20.04 g mannitol, 11.98 g sucrose, 523.5 mg MOPS, 0.5 l milliQ H_2O, pH 7.4), transferred to a glass homogenizer and homogenized for 3 min. Homogenate was then transferred to an ultracentrifuge tube and spun at 300 × g for 10 min at 4 °C. The supernatant was then transferred to a new tube, whereas the pellet was re-homogenized, spun down, and supernatants from the 2 homogenization steps were pooled. The pooled supernatant was then spun at 7000 × g for 10 min at 4 °C to yield the mitochondrial pellet. The supernatant was then discarded, and the pellet was resuspended in MSM buffer, and re-pelleted 2 additional times to rinse the mitochondrial fraction, which was then resuspended in 600 µl MSM buffer. An aliquot was then saved for protein determination, whereas the remaining sample was used for arsenic analysis. Briefly, samples were poured into acid-cleaned 15 ml teflon vials. Concentrated HNO_3 acid (1.5 ml, 15 N), 0.5 ml of ddH_2O, and 5 drops of 30% H_2O_2 were added to the samples, and the vials were sealed. The samples were then heated progressively on a hotplate from 50 to 80 °C for 12 h, while regularly being degassed (after 30 min cooling) until the digestion step was completed. The digested samples were analyzed via a VG Plasmaquad 3 inductively coupled plasma–mass spectrometer.

Larval growth assay. Larval growth assays were performed as previously described (Boyd *et al.*, 2010). Briefly, 25 L1 stage N2, *nuo-6*, *mev-1*, *isp-1*, *isp-1;ctb-1*, *atp-2*, *pyk-1*, *ldh-1*, *ucp-4*, or *bec-1* nematodes were loaded into a 96-well plate using a COPAS Biosort (Union Biometrica Inc., Somerville, MA) (4 wells per strain per treatment). The final volume of each well was then brought to 100 µl with complete EPA water (500 µl 10 mg/ml cholesterol (dissolved in ethanol), 96 mg $NaHCO_3$, 60 mg $MgSO_4{\cdot}7H_2O$, 60 mg $CaSO_4{\cdot}2H_2O$, 4 mg KCl per liter ddH_2O), UVC-killed UvrA, and sodium arsenite to a final concentration of 0, 200, 400, 600, or 800 µM arsenite. Nematodes were then allowed to develop for 48 h at 20 °C. Time of flight ((ToF), a surrogate for nematode length) was then measured using the COPAS Biosort as previously described (Boyd *et al.*, 2010). All experiments were repeated 3 separate times. As all strains do not grow at the same rate, growth data was normalized to percent growth of control (within strain) prior to statistical analysis.

Lethality assay. Ten L4 stage N2, *atg-18*, *bec-1*, *hif-1a* (*ia4* and *ia7*), *sod-1;4;5*, or *sod-2;3* nematodes were loaded into a 96-well plate using a platinum worm pick (2 wells per strain per treatment). The final volume of each well was then brought to 100 µl with complete K-medium, UVC-killed UvrA, and sodium arsenite to a final concentration of 0, 1, 2, 3, 4, 5 mM arsenite. 24 h later, nematodes were scored as dead if they failed to move in response to repeated probing with a platinum worm pick. All experiments were repeated 3 separate times.

PDH activity assay. PDH activity was measured in isolated mitochondria following 48 h of arsenite exposure using a Pyruvate Dehydrogenase Activity Colorimetric Assay Kit (BioVision, Cat. # K679). Mitochondria were isolated as described above, and resuspended in BioVision's PDH Assay Buffer. PDH activity was then measured following manufacturer's instructions. All experiments were repeated 3 separate times.

Mitochondrial membrane potential. Mitochondrial membrane potential was measured using the dual-emission potential-sensitive dye JC-1 (Sigma–Aldrich), which fluoresces red with high membrane potential, and green at lower membrane potential. Briefly, 3 µM JC-1 (dissolved in 1% DMSO) was added to control and arsenite-exposed nematodes for the final 12 h of arsenite exposure. Following the exposure, nematodes were rinsed 3–4 times, and allowed to clear their guts. Nematodes were then placed on a 10% agar pad with 100 mM levamisole (paralytic used for imaging) and imaged on a Zeiss 510 upright confocal microscope using a 63× water-immersion objective (Light Microscopy Core Facility, Duke University). To standardize the mitochondrial population assayed, the posterior pharyngeal bulb was chosen as the region of interest. Red and green pixel intensities within this anatomically identifiable area were measured using ImageJ. A 1 h exposure to 50 µM FCCP (2% DMSO) was used as a positive control. Four nematodes were imaged per experiment, which was repeated 2 separate times.

Statistics. All statistical analysis was performed using JMP v11.0 software (SAS Institute). All data was initially assessed using a 1 or 2 way ANOVA, and when warranted post-hoc analysis was performed using Tukey's Honest Significant Difference test.

RESULTS

Trivalent arsenite was used in all experiments because it is one of the predominant arsenicals found in groundwater and is generally more toxic than pentavalent arsenate (Hughes, 2002). As we were primarily interested in investigating the mitochondrial effects of arsenite in somatic tissues, and development of the nematode germline is associated with dramatic changes in mitochondrial biology (including increased OXPHOS and mtDNA copy number) that could confound our results, we used germline-deficient PE255 *glp-4* or *glp-1* nematodes for all experiments.

Arsenite Increases Glycolysis and Reduces the Function of ETC Complexes II and V. To rapidly test for altered mitochondrial function in response to arsenite exposure, we developed a novel assay that permits *in vivo* assessment of the relative degree of chemical-induced inhibition of different metabolic processes (eg, OXPHOS and glycolysis) that contribute to the maintenance of steady-state ATP levels (Luz *et al.*, 2016). Transgenic, luciferase-expressing, PE255 *glp-4* nematodes were exposed to 0, 50, 250, or 500 µM arsenite. Although these concentrations of arsenite fall below the previously reported nematode 24 h LC_{50} value of 1.3 mM (Tseng *et al.*, 2007), some mortality was observed in PE255 *glp-4* nematodes exposed to the highest concentration of arsenite (500 µM, qualitative observation, A. Luz). Therefore, this concentration was not used with PE255 *glp-4* nematodes. Transgenic PE255 nematodes express ATP-powered firefly luciferase, which allows for the rapid, *in vivo* determination of steady-state ATP levels (Lagido *et al.*, 2015; Lagido *et al.*, 2008); thus, after 48 h of arsenite exposure we measured real-time changes in ATP levels after short-term (1, 3, or 4.5 h) exposure to various inhibitors of the ETC, glycolysis, or the Krebs cycle (Table 1). The principal that underlies this assay is that differential depletion of ATP indicates altered function (defined here as maintenance of steady-state *in vivo* ATP levels) at the site of inhibition in response to arsenite exposure. For example,

if inhibition of complex I normally results in a decrease in ATP levels of 70%, but after arsenite exposure the same inhibition results in a decrease of only 35%, this suggests that arsenite exposure is reducing complex I function, and thus its overall contribution to steady-state ATP levels.

Steady-state ATP levels were reduced in a dose-dependent manner following a 48 h arsenite exposure (1 way ANOVA, $P < .0001$) (Figure 1A). To assess the relative contributions of different metabolic processes that contribute to the maintenance of ATP levels, we normalized ATP levels after each inhibitor to the appropriate EPA H_2O (2-DG, DCA), 1% DMSO (rotenone, TTFA, antimycin A, DCCD), or 2% DMSO (FCCP) controls. 2% DMSO (1 h exposure) had no significant effect on ATP levels (1 way ANOVA, $P = .25$); however, 1% DMSO (3 h exposure) did cause a small, but significant reduction (~16%) in ATP levels in nematodes exposed to 250 μM arsenite (1 way ANOVA, $P = .009$) (Figure 1B and C).

Arsenite exposure had no effect on ETC complex III (1 way ANOVA, $P = .75$), IV (1 way ANOVA, $P = .99$) or pyruvate dehydrogenase kinase (1 way ANOVA, $P = .20$) activities (Supplemental Figure S1A–C). The apparent trend towards reduced complex I activity (ie, reduced sensitivity to ATP depletion following rotenone exposure) observed following arsenite exposure was not statistically significant (1 way ANOVA, $P = .069$) (Figure 1D). Interestingly, reduced complex II activity was observed in nematodes exposed to both 50 and 250 μM arsenite (1 way ANOVA, $P < .0001$; $P = .030$ and $P < .0001$, respectively, for pairwise comparisons to control) (Figure 1E), whereas only 250 μM arsenite reduced ATP synthase activity (1 way ANOVA, $P < .0001$; $P < .0001$ for pairwise comparison to control) (Figure 1F). Furthermore, 50, but not 250 μM arsenite reduced nematode sensitivity to ATP depletion following exposure to the mitochondrial uncoupler FCCP (1 way ANOVA, $P = .038$; $P = .045$) and $P = .090$, respectively, for pair-wise comparisons to control) (Figure 1G), whereas inhibition of glycolysis with 2-DG reduced ATP levels in nematodes exposed to both 50 and 250 μM arsenite (1 way ANOVA, $P = .017$; $P = .049$ and $P = .017$, respectively, for pairwise comparisons to control) (Figure 1H).

Although reduced ATP depletion following TTFA, DCCD, and FCCP exposure in arsenite treated nematodes may be due to compensatory increases in ATP production via alternative routes such as glycolysis, we do not expect this to be the case. If compensatory increases in glycolysis were maintaining ATP levels, then all ETC inhibitors should elicit smaller reductions in ATP in the context of arsenite exposure. Collectively, these results indicate that arsenite disrupted OXPHOS and induced aerobic glycolysis, suggesting the induction of a Warburg-like effect.

Arsenite Disrupts Pyruvate Metabolism. To further characterize the metabolic details and time course of the observed shift from OXPHOS to aerobic glycolysis in transgenic PE255 *glp-4* nematodes, we quantified metabolites important to energy production following 12, 24, and 48 h of 0, 50, or 500 μM arsenite exposure using non-transgenic, germline-deficient *glp-1* nematodes. Interestingly, *glp-1* nematodes exposed to 500 μM arsenite appeared quite healthy and no mortality was observed (qualitative observation, A. Luz); thus, as with the previous experiment, the highest concentration of arsenite (500 μM) tested was chosen based on the fact that it caused no mortality. Mean metabolite concentrations, as well as $\log_2$ fold change, standard error, and *P*-values for all statistical analyses are listed in Supplemental File 1.

Exposure to 500 μM arsenite resulted in the accumulation of pyruvate after 12 (1 way ANOVA, $P = .0088$), 24 (1 way ANOVA, $P = .0011$), and 48 h (1 way ANOVA, $P = .0002$) of arsenite exposure (Figure 2A), whereas lactate only accumulated detectably following 48 h of exposure (1 way ANOVA, $P = .048$) (Figure 2B). No Krebs cycle intermediates were significantly altered in response to arsenite exposure, though trends in reduced citrate (1 way ANOVA, $P = .056$), and increased malate (1 way ANOVA, $P = .085$) were observed following 24 and 48 h of arsenite exposure, respectively (Supplemental File 1), suggesting mild disruption of Krebs cycle activity. Because these results suggest that arsenite disrupted pyruvate metabolism, we measured pyruvate dehydrogenase (PDH) activity after 48 h of arsenite exposure, and found a dose-dependent reduction in PDH activity (1 way ANOVA, $P = .0016$) (Figure 2C).

Because amino acid catabolism can fuel energy metabolism, we quantified amino acid levels following arsenite exposure. Glycine, the only amino acid altered after 12 h of exposure, was elevated (1 way ANOVA, $P = .014$), whereas aspartate/asparagine (1 way ANOVA, $P = .044$), glycine (1 way ANOVA, $P = .035$), and valine (1 way ANOVA, $P = .045$) were all elevated following 24 h of exposure to 500 μM arsenite (Supplemental File 1). Interestingly, 11 amino acids (Ala, Asx, Cit, Glx, Gly, His, Leu/Ile, Orn, Ser, Tyr, Val) were elevated following 48 h of exposure to 50 and/or 500 μM arsenite (1 way ANOVA's for each amino acid, $P < .05$, as listed in Supplemental File 1), whereas non-statistically significant trends in the same direction (increased) were also observed for arginine (1 way ANOVA, $P = .070$), methionine (1 way ANOVA, $P = .061$), and phenylalanine (1 way ANOVA, $P = .054$) (Figure 3). This amino acid profile is consistent with increased autophagy and/or proteasomal degradation in response to arsenite exposure, as previously reported *in vitro* (Bolt *et al.*, 2010; Zhang *et al.*, 2012). Using a genetic approach, we carried out additional experiments to test for a functional role for autophagy in tolerating arsenic toxicity. Autophagy protects against arsenic toxicity: *bec-1*-deficient nematodes are mildly, yet statistically significantly sensitive to arsenite exposure (2 way ANOVA, main effects of strain ($P < .0001$), arsenite ($P < .0001$), and their interaction ($P = .013$)) in a 48 h larval growth assay (Supplemental Figure S2) and in a 24 h lethality assay (Supplemental Figure S3), whereas *atg-18*-deficient nematodes are highly sensitive to arsenite (2 way ANOVA, main effects of strain, arsenite and their interaction ($P < .0001$ for all) Supplemental Figure S3).

Because these results suggest an induction of autophagy following arsenite exposure, we hypothesized that increased autophagy might lead to increased mitochondrial turnover, and thus possibly altered mtDNA copy number (assuming no compensatory change in biogenesis). However, no significant changes in mtDNA (1 way ANOVA, $P = .15$), nucDNA (1 way ANOVA, $P = .99$), or their ratio (1 way ANOVA, $P = .87$) were observed following 48 h of arsenite exposure (Supplemental Figure S4A–C).

Interestingly, a 2-fold increase in alanine was observed in nematodes exposed to both 50 and 500 μM arsenite (Figure 3), which could result from increased transamination of pyruvate to alanine, further suggesting a disruption of pyruvate metabolism. Likewise, large increases in citrulline and ornithine were observed (Figure 3), suggesting disruption of the urea cycle; however, functional urea cycle enzymes are yet to be identified in *C. elegans* (Falk *et al.*, 2008).

Acetyl-CoA can also enter the Krebs cycle, fueling energy metabolism, through β-oxidation of fatty acids. Thus, we quantified acylcarnitine levels, a biomarker of acyl-CoA species (Liu

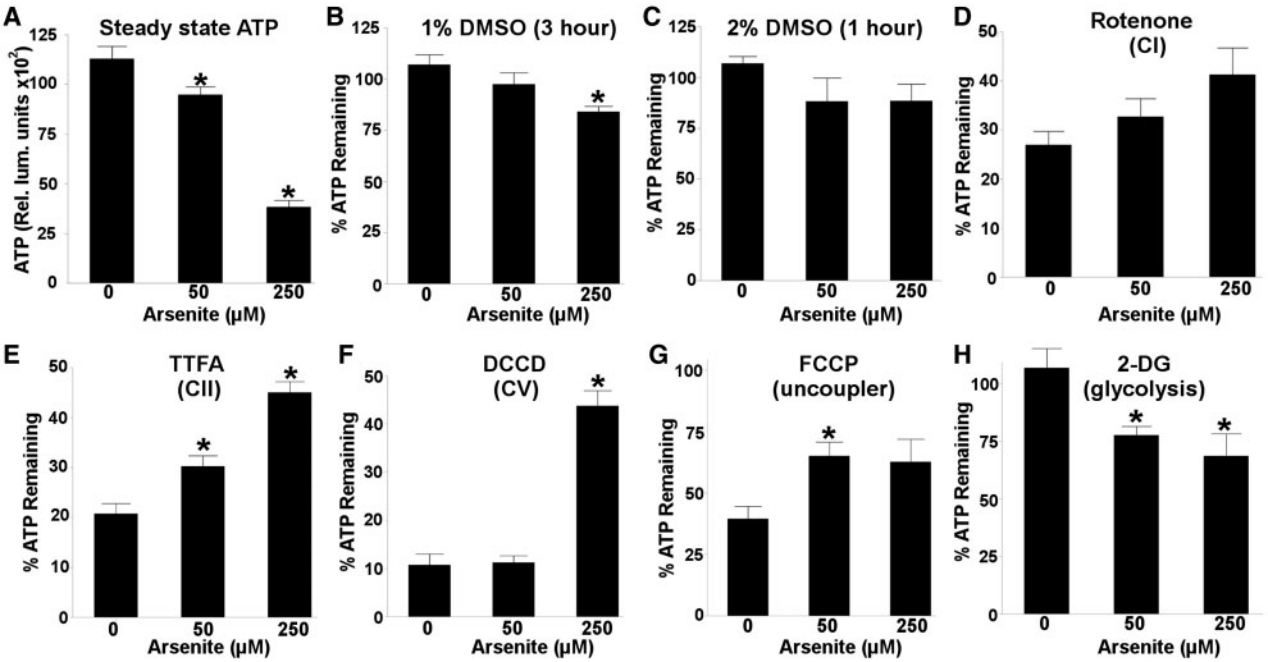

FIG. 1. Arsenite disrupts the mitochondrial ETC and induces glycolysis. B–H, the percent ATP remaining in arsenite treated nematodes after exposure to the vehicle control or various metabolic inhibitors. Higher percent ATP remaining indicates a reduced role in steady state ATP maintenance, and thus reduced activity, for the complex being inhibited. **(A)** A 48 h exposure to arsenite reduced steady-state ATP levels in a dose-dependent manner (one way ANOVA, $P < 0.0001$). Exposure to **(B)** 1% DMSO (3 h exposure) caused a slight reduction (16%) in ATP in nematodes exposed to 250 μM arsenite (one way ANOVA, $P = 0.0085$); however, no sensitivity to **(C)** 2% DMSO (1 h exposure) was observed (one way ANOVA, $P = 0.25$). A trend in reduced **(D)** complex I activity was observed in nematodes exposed to arsenite (one way ANOVA, $P = 0.069$), while arsenite reduced the activity of **(E)** complex II (one way ANOVA, $P < 0.0001$), **(F)** ATP synthase (one way ANOVA, $P < 0.0001$), and reduced sensitivity to (G) mitochondrial uncoupling (one way ANOVA, $P = 0.038$), whereas increasing (H) glycolysis (one way ANOVA, $P = 0.017$). Asterisk denotes statistical significance ($P < 0.05$) for post-hoc comparison (Tukey's HSD) to control. $N = 4$–6. Bars ± SEM.

et al., 2015), following arsenite exposure. Levels of several short (C3, C5, C5-OH/C3-DC, C6, C6-DC/C8-OH, C8) and medium chain (C14:1, C14:2) acylcarnitines were mildly increased following exposure to arsenite (Supplemental File 1). However, arsenite exposure did not alter any long chain acylcarnitines, suggesting arsenite has minimal effect on fatty acid oxidation.

Arsenite Reduces ATP Content, ATP-Linked Respiration, and Spare Respiratory Capacity, While Increasing Proton Leak. Because the majority of alterations in metabolites (ie, amino acids, pyruvate, and lactate) were observed following 48 h of arsenite exposure, we characterized the functional consequences of these alterations on mitochondrial respiration (basal OCR, spare respiratory capacity (SRC), ATP-linked respiration, and proton leak) using the Seahorse XF^e Bioanalyzer after 48 h of arsenite exposure in *glp-1* nematodes.

Unexpectedly, basal OCR was not significantly altered by arsenite exposure (Figure 4A) (1 way ANOVA, $P = .061$). However, ATP levels were significantly reduced by 50, but not 500 μM arsenite (Figure 4B) (1 way ANOVA, $P = .042$; $P = .032$ for pairwise comparisons to control). Interestingly, a dose dependent reduction in ATP-linked respiration (Figure 4C) (1 way ANOVA, $P < .0001$; $P < .0001$ for both pairwise comparisons to control) and increase in proton leak were observed following arsenite exposure (Figure 4E) (1 way ANOVA, $P < .0001$; $P < .0001$ for both pairwise comparisons to control), whereas both 50 and 500 μM arsenite severely reduced spare respiratory capacity (Figure 4D) (1 way ANOVA, $P < .0001$; $P < .0001$ and $P = .0001$, respectively, for pairwise comparisons to control). Arsenite altered mitochondrial respiration in a similar manner (eg, increased proton leak, and reduced ATP-linked respiration and spare capacity) in PE255 *glp-4* nematodes (Supplemental Figure S5A–D), demonstrating that arsenite induced similar alterations in mitochondrial respiration in both genetic backgrounds.

To further test the role of proton leak, which is defined as the transport of protons across the inner mitochondrial membrane independent of ATP synthase activity, we measured mitochondrial membrane potential, which should be reduced by mitochondrial uncoupling, using the potential-sensitive dye JC-1. As expected, arsenite reduced mitochondrial membrane potential (1 way ANOVA, $P = .0023$) (Figure 5A–E). Next, we tested whether nematodes deficient in mitochondrial (*sod-2;3*) and non-mitochondrial (*sod-1;4;5*) superoxide dismutase would be sensitive to arsenite, as the activity of mitochondrial uncoupling proteins can be induced by ROS. Both *sod-2;3*- and *sod-1;4;5*-deficient nematode strains were sensitive to arsenite (2 way ANOVA, main effects of strain, arsenite, and their interaction ($P < .0001$ for all)) (Supplemental Figure S6). Finally, we tested for arsenite sensitivity in nematodes deficient in *ucp-4* (the sole mitochondrial uncoupling protein homolog in nematodes). No sensitivity was observed compared with wild-type (N2) nematodes (2 way ANOVA, main effect of arsenite ($P < .0001$), but not strain ($P = .057$), or their interaction ($P = .47$)) (Supplemental Figure S7). However, this may be explained by the fact that *ucp-4* has been shown to play a role in succinate transport, and does not appear to function as a classical uncoupler in nematodes (Pfeiffer *et al.*, 2011).

Because the arsenite-induced metabolic shift from oxidative phosphorylation to glycolysis has been shown to be dependent upon HIF-1A stabilization in several cell lines (Zhao *et al.*, 2013), we next tested whether *hif-1α*-deficient nematodes would be sensitive to arsenite. However, no sensitivity was observed in 2

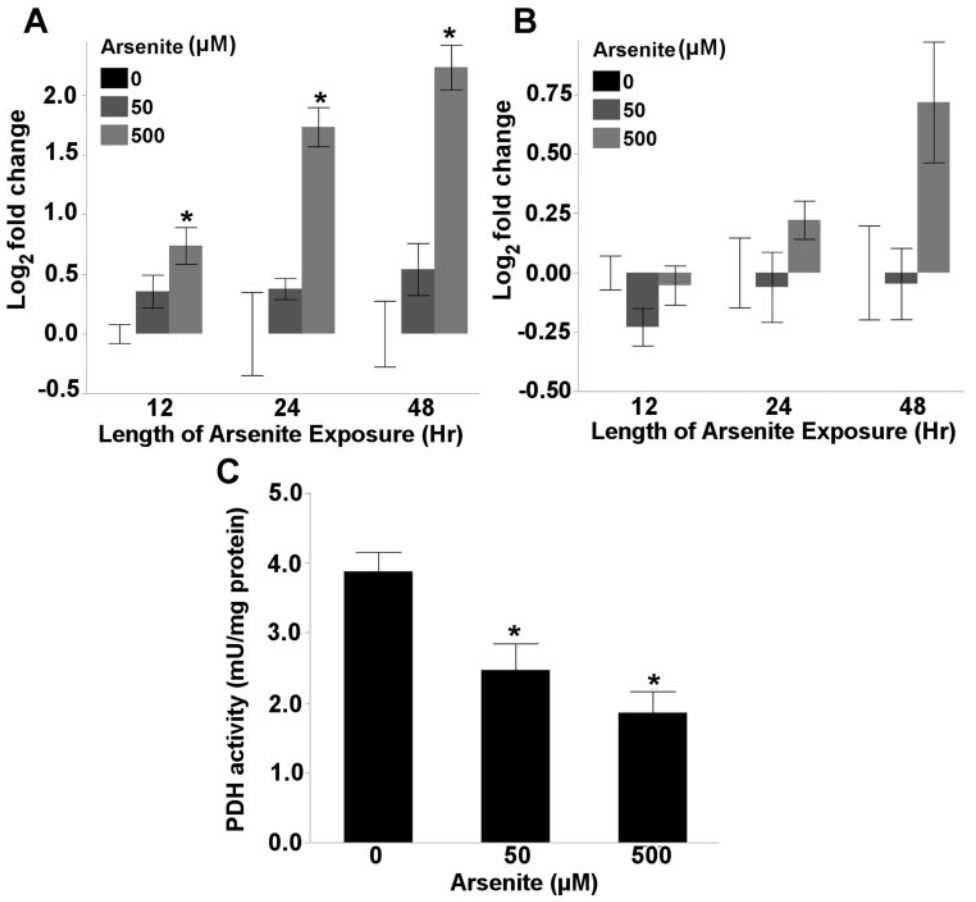

FIG. 2. Arsenite disrupts pyruvate metabolism. Exposure to 500 μM arsenite resulted in the accumulation of (A) pyruvate after 12 (one way ANOVA, $P = 0.0088$), 24 (one way ANOVA, $P = 0.0011$), and 48 h (one way ANOVA, $P = 0.0002$) of exposure; whereas (B) lactate levels were only effected after 48 h of arsenite exposure (one way ANOVA, $P = 0.048$). Alternatively, exposure to both 50 and 500 μM arsenite reduced pyruvate dehydrogenase (PDH) activity after 48 h of exposure (one way ANOVA, $P = 0.0016$). Asterisk denotes statistical significance ($P < 0.05$) for post-hoc comparison (Tukey's HSD) to control within each time point. $N = 4$–6. Bars ± SEM.

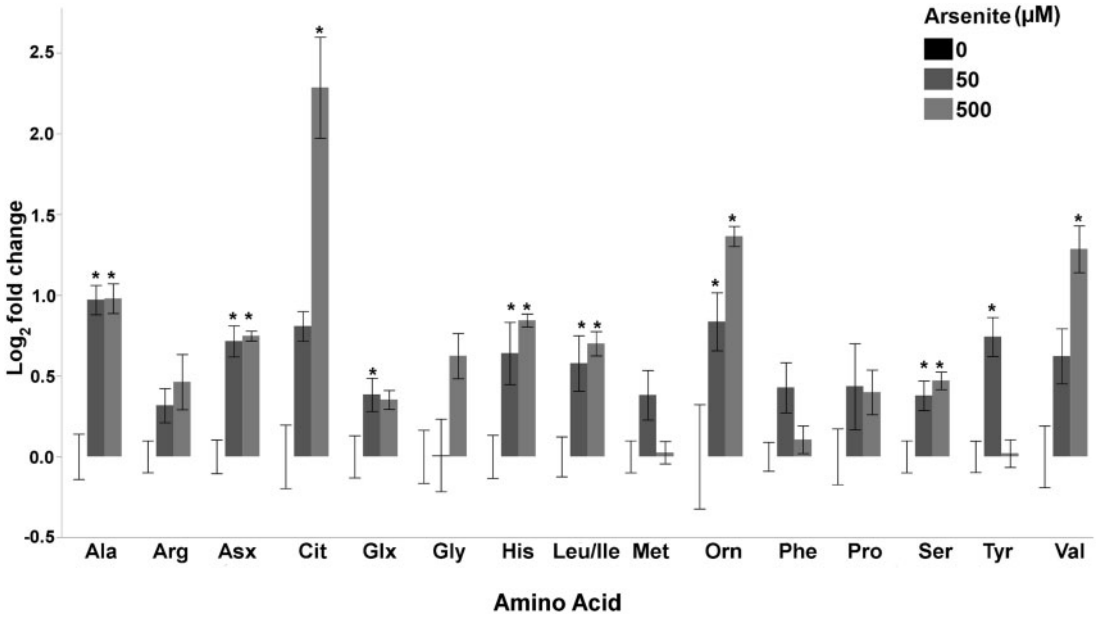

FIG. 3. Arsenite alters amino acid levels. Amino acid levels were elevated following 48 h of exposure to arsenite. Asterisk denotes statistical significance ($P < 0.05$) for post-hoc comparison (Tukey's HSD) to control. $N = 5$. Bars ± SEM.

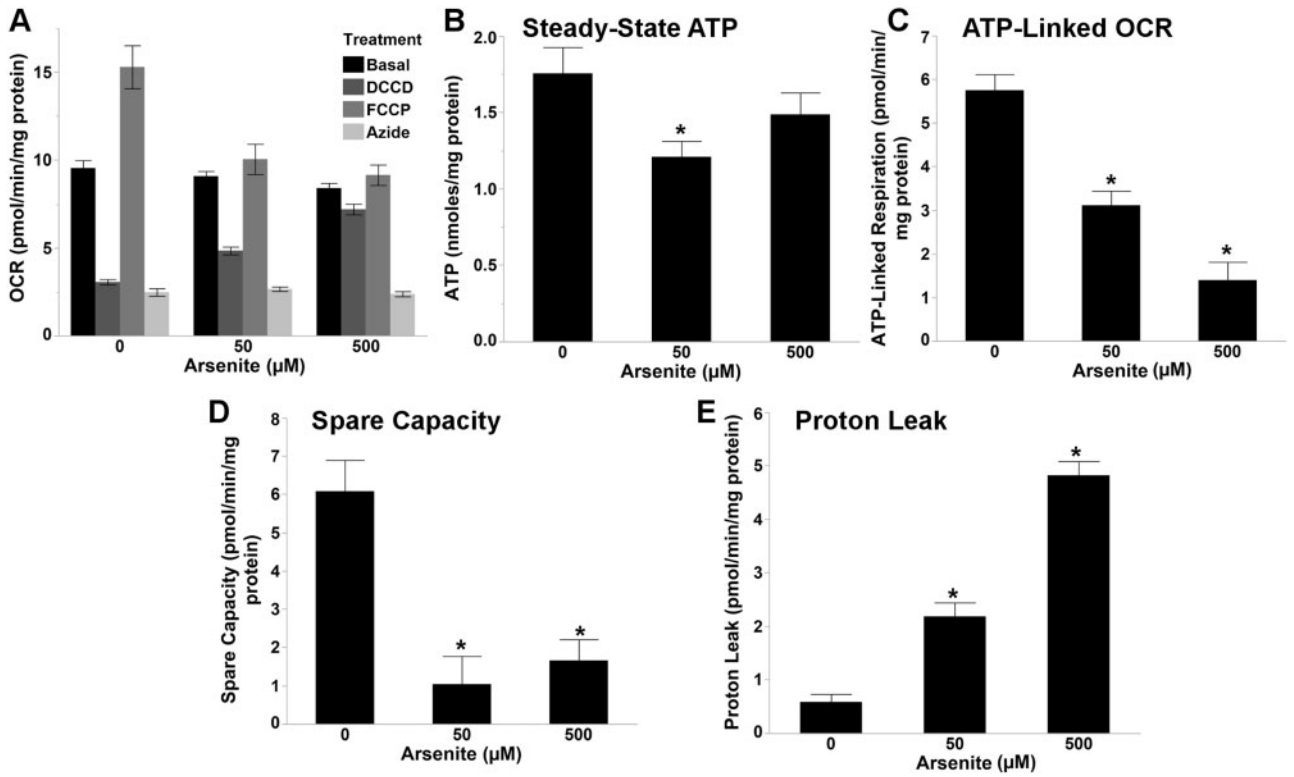

FIG. 4. Arsenite disrupts mitochondrial respiration. **(A)** Metabolic profile obtained via Seahorse XF^{e}24 analysis following a 48 h exposure to arsenite. Arsenite reduced **(B)** ATP levels (one way ANOVA, $P = 0.042$, $N = 9$–12), **(C)** ATP-linked respiration (one way ANOVA, $P < 0.0001$, $N = 22$), **(D)** spare respiratory capacity (one way ANOVA, $P < 0.0001$, $N = 22$), and increased **(E)** proton leak (one way ANOVA, $P < 0.0001$, $N = 22$) in *glp-1* nematodes. Asterisk denotes statistical significance ($P < 0.05$) for post-hoc (Tukey's HSD) comparison to control. Bars ± SEM.

different hif-1α-deficient strains (2 way ANOVA, main effect of arsenite ($P < .0001$), but not strain or their interaction ($P > .05$ for both)) (Supplemental Figure S8).

Mutations in ETC and Glycolytic Genes Sensitize Nematodes to Arsenite Toxicity. Because both high and low concentrations of arsenite severely disrupted mitochondrial respiration and induced aerobic glycolysis, we hypothesized that mutations in glycolytic genes and various complexes of the ETC, which cause mitochondrial disease in humans (DiMauro and Schon, 2003), would sensitize nematodes to arsenite toxicity. In support of our hypothesis, deficiencies in pyruvate kinase and lactate dehydrogenase sensitized nematodes to arsenite toxicity in a larval growth assay (2 way ANOVA, main effects of arsenite, strain and their interaction ($P < .0001$ for all)) (Figure 6A), whereas deficiencies in ETC complexes I, II, and III, but not ATP synthase, also sensitize nematodes to arsenite toxicity (2 way ANOVA, main effects of arsenite, strain and their interaction ($P < .0001$ for all)) (Figure 6B). Because many of these genetically deficient strains develop at reduced rates, all time of flight (ToF, a surrogate measure of nematode length) data was normalized to percent growth of control for statistical analysis (Figure 6; raw ToF data is shown in Supplemental Figs. S9 and S10).

Accumulation of Arsenite in Nematode Mitochondria Is Comparable to Arsenite Accumulation in Low-Dose In Vitro Studies. Because the concentrations of arsenite used in this study are high compared with cell culture studies, we quantified the amount of arsenite accumulating in nematode mitochondria to determine if the concentrations of arsenite used in this study are comparable to low-dose (75 ppb) *in vitro* studies that elicit similar effects. Concentrations of arsenite in isolated mitochondria were 63.0 ± 6.5 and 330.1 ± 6.7 ng arsenic per mg mitochondrial protein following 48 h exposure to 50 and 500 μM arsenite, respectively (Supplemental Figure S11), which, at least for 50 μM, is comparable to concentrations of arsenite measured in mitochondria isolated from low-dose *in vitro* studies (Naranmandura *et al.*, 2011).

DISCUSSION

Despite decades of research studying the toxic effects of arsenic, the mechanism by which arsenic causes cancer and other diseases remains poorly understood. Recently, arsenite was shown to induce aerobic glycolysis *in vitro* (Zhao *et al.*, 2013), implicating metabolic dysfunction in arsenic-induced disease. Here, using the model organism, *C. elegans*, we demonstrate that arsenite can induce glycolysis *in vivo*. Furthermore, we report for the first time arsenite-induced alterations in mitochondrial function, including reduced ATP-linked respiration and spare respiratory capacity, as well as increased proton leak. Finally, we report that deficiencies in the mitochondrial ETC, which cause disease in humans, sensitize nematodes to arsenite exposure, thus identifying a novel class of gene-environment interactions that warrant further investigation in the human populace.

Arsenite-induced aerobic glycolysis *in vitro* is dependent upon the stabilization of HIF-1A (Li *et al.*, 2014; Zhao *et al.*, 2014, 2013), a transcription factor that regulates expression of genes involved in glycolysis, and Krebs cycle activity (ie, PDHK, a negative regulator of PDH) under hypoxic conditions (Kim *et al.*, 2006). Under oxygen replete conditions HIF-1A is constitutively

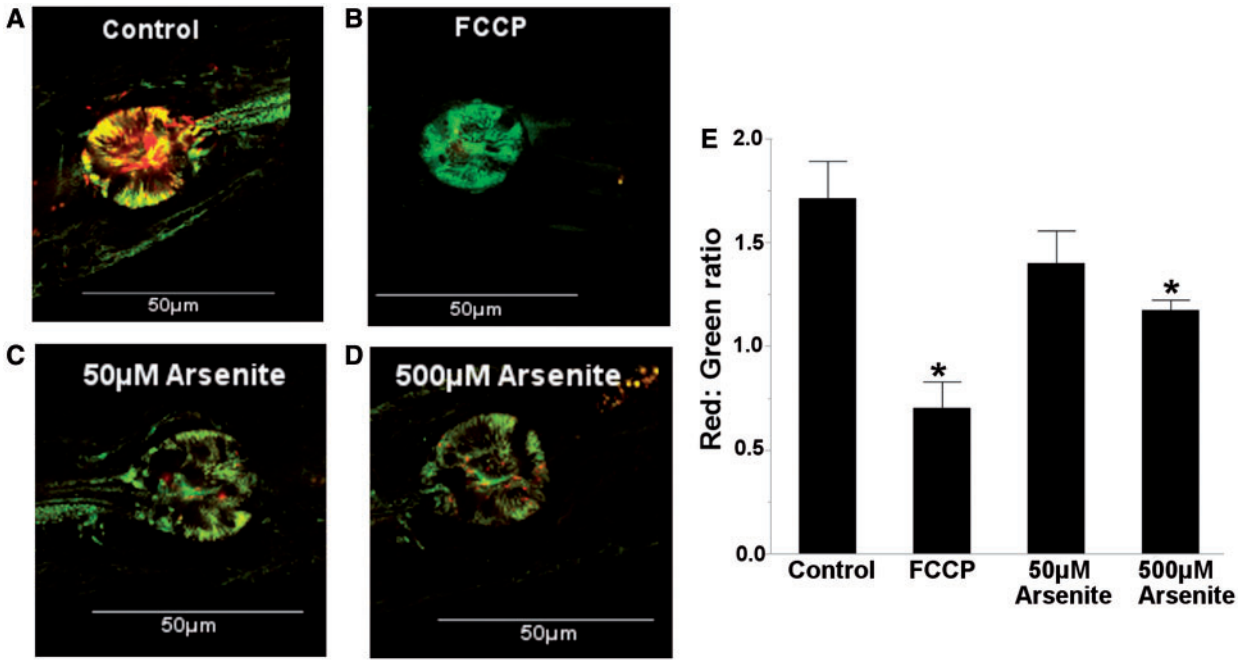

FIG. 5. Arsenite reduces mitochondrial membrane potential. The ratio of red to green fluorescence intensity was measured in the posterior pharyngeal bulb of **(A)** control, **(B)** 50 µM FCCP (positive control), **(C)** 50 µM arsenite, and **(D)** 500 µM arsenite exposed nematodes. **(E)** Arsenite reduced mitochondrial membrane potential in a concentration dependent manner (one way ANOVA, $P = 0.0023$). A–D, representative images of JC-1 staining. Asterisk denotes statistical significance ($P < 0.05$) for post-hoc (Tukey's HSD) comparison to control. $N = 8$. Bars ± SEM. Please see online version to view figure in color.

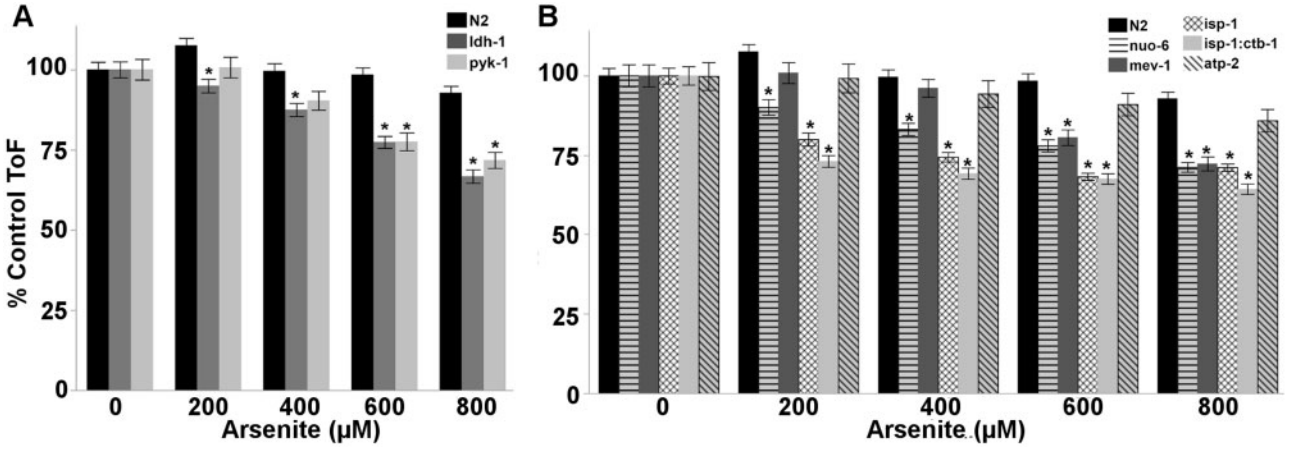

FIG. 6. Deficiencies in glycolysis and ETC genes sensitize nematodes to arsenite. Nematodes deficient in **(A)** pyruvate kinase and lactate dehydrogenase (two way ANOVA, main effects of strain, arsenite and their interaction ($P < 0.0001$ for all)), as well as **(B)** ETC complexes I (*nuo-6*), II (*mev-1*), and III (*isp-1*; *isp-1*:*ctb-1*), but not ATP synthase (*atp-2*), are sensitive to arsenite exposure (two way ANOVA, main effects of strain, arsenite and their interaction ($P < 0.0001$ for all)) in a 48 h larval growth assay. As nematode strains develop at varying rates, all ToF (surrogate for nematode length) data is normalized to percent growth of control. Raw ToF data is shown in Supplemental Figures S9 and S10. Asterisk denotes statistical significance ($P < 0.05$) for post-hoc (Tukey's HSD) comparison to N2 within each arsenite concentration, and are listed in Supplemental File 1. $N = 166$–406. Bars ± SEM.

targeted for proteasomal degradation via the action of prolyl hydroxylase domain (PHD) proteins and von Hippel Lindau proteins (Ke and Costa, 2006). Arsenite-induced ROS can deplete redox-sensitive ascorbate, a cofactor required for PHD function, leading to HIF-1A accumulation under oxygen replete conditions (Li *et al.*, 2014), an induction of aerobic glycolysis (Zhao *et al.*, 2013), and a loss of anchorage dependent cell growth (Zhao *et al.*, 2014). However, HIF-1A does not appear to be playing a role in the observed Warburg-like effect in nematodes, as HIF-1A-deficient strains were not sensitive to arsenite compared with wild type nematodes. Instead, the rapid disruption of pyruvate metabolism is likely due to reduced PDH activity. Because arsenite is a well-known inhibitor of PDH (Bergquist *et al.*, 2009), direct enzyme inhibition could be responsible for reduced PDH activity; however, high intracellular ratios of ATP:ADP, acetyl-CoA:CoA, and NADH:NAD^+ can also inhibit PDH activity, and cannot be ruled out.

Unexpectedly, arsenite did not alter basal respiration despite a dose-dependent reduction in ATP-linked respiration. This is surprising, as steady-state ATP levels were only reduced in nematodes exposed to 50 µM arsenite. This suggests that an alternative pathway, such as glycolysis, is maintaining steady-

state ATP levels. In agreement with this, 2-DG reduced steady-state ATP levels in *glp-4* nematodes exposed to both 50 and 250 μM arsenite; however, pyruvate and lactate only accumulated in *glp-1* nematodes exposed to the highest concentration of arsenite. This could indicate a more robust induction of glycolysis, capable of maintaining ATP levels, in the highest exposure group. Alternatively, limited lactate accumulation in nematodes could be explained by the presence of a pathway homologous to the mammalian Cori cycle, which converts lactate to glucose in the liver under periods of high energy demand. Although this pathway has not yet been confirmed, the *C. elegans* genome contains a monocarboxylate transporter homolog (K05B2.5), which functions as a lactate transporter in the mammalian Cori cycle (Hope *et al.*, 1998). Interestingly, under anoxic conditions, nematodes do not appear to accumulate lactate in their tissues. Instead, excess lactate is excreted or converted to ethanol and then excreted (Cooper and Van Gundy, 1971; Föll *et al.*, 1999), which could also explain why lactate did not accumulate in nematodes exposed to lower concentrations of arsenite.

Arsenite exposure induced a dose-dependent increase in proton leak, which is catalyzed biologically in part via the action of uncoupling proteins, whose activity can be induced via superoxide, fatty acid anions, and by-products of lipid peroxidation. Thus, inducible proton leak can function to limit further mitochondrial ROS production through a negative feedback loop (Brand *et al.*, 2004). Indeed, reduced mitochondrial membrane potential following arsenite exposure is supportive of mitochondrial uncoupling. However, consistent with previous reports that *ucp-4*, the single known *C. elegans* uncoupling protein homolog, does not function as a classical uncoupler (Pfeiffer *et al.*, 2011), *ucp-4*-deficient nematodes were not sensitive to arsenite exposure, compared with wild type nematodes. The fact that both mitochondrial (*sod-2;3*) and non-mitochondrial (*sod-1;4;5*) superoxide dismutase-deficient nematodes were sensitive to arsenite provides evidence of arsenite-induced superoxide production, which could then induce proton leak through other mitochondrial carriers, such as the adenine nucleotide translocator or dicarboxylate carrier, which facilitates fatty acid-mediated proton transport (Wię and Wojtczak, 1997). In support of this, arsenite has previously been shown to induce ANT channel activity *in vitro* (Belzacq *et al.*, 2001).

Spare respiratory capacity was severely reduced by both 50 and 500 μM arsenite. This could be explained by the fact that mitochondrial respiration is already uncoupled by arsenite, thus limiting further uncoupling by FCCP. Furthermore, arsenite exposed nematodes were less sensitive to ATP depletion in the presence of the mitochondrial uncoupler, FCCP, which further supports arsenite-induced mitochondrial uncoupling, and an alternative, non-oxidative, means of ATP production. Alternatively, arsenite may reduce SRC by directly inhibiting complexes of the ETC or by reducing Krebs cycle activity, thus limiting ETC substrate (NADH, $FADH_2$). However, only methylated trivalent arsenicals (MMA and DMA) have been shown to directly inhibit the ETC (Naranmandura *et al.*, 2011), and as the nematode genome lacks an AS3MT homolog (Thomas *et al.*, 2007), direct inhibition seems unlikely. Finally, although the accumulation of pyruvate suggests reduced flow of pyruvate into the Krebs cycle, and thus reduced Krebs cycle activity, no Krebs cycle intermediates were significantly altered by arsenite exposure, ostensibly eliminating substrate limitation as causative of reduced SRC.

In addition to the oxidation of glucose, the oxidation of fatty acids and amino acids can also fuel mitochondrial respiration. However, only minor changes in acylcarnitine levels, a biomarker of acyl-CoA species (Liu *et al.*, 2015), were observed following arsenite exposure, suggesting arsenite has minimal effects on fatty acid oxidation. Interestingly, both 50 and 500 μM arsenite significantly increased the levels of a majority of amino acids (10/15), a change consistent with increased autophagy and/or proteasomal degradation. This is further supported by the fact that *bec-1*- and *atg-18*-deficient nematodes are sensitive to arsenite exposure. Arsenite induced autophagy is not surprising, as arsenite has high affinity for protein thiols (Kitchin and Wallace, 2008), and thiol binding has been shown to cause protein misfolding (Cline *et al.*, 2003) and subsequent proteasomal (Bergquist *et al.*, 2009) and lysosomal degradation (Myeku and Figueiredo-Pereira, 2011). Furthermore, the accumulation of ubiquitin-conjugated proteins (Kirkpatrick *et al.*, 2003), and the induction of autophagy (Bolt *et al.*, 2010; Zhang *et al.*, 2012) following arsenite exposure have previously been reported *in vitro*. Alternatively, alanine, ornithine, and citrulline appear to be the amino acids most affected by arsenite exposure. This further suggests altered pyruvate metabolism (ie, increased transamination of pyruvate to alanine), and/or disruption of the urea cycle, or the nematode equivalent, as nematodes appear to lack functional urea cycle enzymes (Falk *et al.*, 2008).

Genetic variation is associated with altered arsenic-induced disease and cancer risk (Lesseur *et al.*, 2012). However, little is currently known about how individuals suffering from mitochondrial disease will respond to arsenite exposure. We were concerned that individuals suffering from mitochondrial disease could represent a large subpopulation displaying increased sensitivity to arsenite, as collectively, an estimated 1 in 4000 individuals suffer from mitochondrial disease (Schaefer *et al.*, 2004). Indeed, we observed increased arsenite sensitivity in nematodes deficient in ETC complex I (*nuo-6*), II (*mev-1*), and III (*isp-1, isp-1;ctb-1*), but not V (*atp-2*). *nuo-6*, *isp-1*, *isp-1;ctb-1*, and *atp-2* nematodes are long-lived and ROS-resistant, whereas *mev-1* nematodes are short-lived and ROS-sensitive (Kondo *et al.*, 2005; Tsang *et al.*, 2001; Yang and Hekimi, 2010). Interestingly, many ETC mutants upregulate the activity of other ETC complexes to survive, for example complex I mutants have been shown to upregulate complex II (Morgan *et al.*, 2015). Thus, it is likely that reduced metabolic plasticity in the context of arsenite-induced inhibition of complexes I, II, and V (Figure 1), and not hypersensitivity to ROS, underlies the observed genetic sensitization to arsenite toxicity. Interestingly, previous studies have shown mild uncoupling in yeast and *Chlamydomonas* carrying ATP-synthase deficiencies (Lapaille *et al.*, 2010; Wang *et al.*, 2007), which may help to limit arsenite toxicity in *atp-2*-deficient nematodes.

Presently, it is unclear why PE255 *glp-4* nematodes are more sensitive to arsenite than *glp-1* nematodes. Although mutations in both genes result in similar germline phenotypes, they participate in different molecular processes: *glp-1* encodes a notch receptor ligand (Yochem and Greenwald, 1989), whereas *glp-4* encodes a valyl aminoacyl tRNA synthetase (Rastogi *et al.*, 2015). This raises the possibility that *glp-4* plays a role in arsenic-related toxicity. However, we have previously reported a similar differential sensitivity between the two strains to 5-fluoro-2′-deoxyuridine (DNA synthesis inhibitor) (Rooney *et al.*, 2014), and have observed the same for rotenone and paraquat (unpublished observations). Furthermore, arsenic induces similar alterations in mitochondrial respiration between the 2 strains (ie, increased proton leak, and reduced ATP-linked OCR and spare capacity). These results demonstrate that increased sensitivity

in *glp*-4 nematodes is not limited to arsenite, and that arsenite induces similar trends in mitochondrial dysfunction between the two strains.

Although the concentrations of arsenite used in this study are high (3.75 and 37.5 ppm), drinking water arsenic concentrations in the 1–5 ppm range have been measured in Argentina, Bangladesh, Chile, Thailand, Vietnam, and West Bengal (Rahman, 2002). More importantly with regard to the relevance of our study, nematodes display some of the lowest sensitivity to arsenic yet observed, with a previously reported 24 h LC_{50} value of 1.3 mM arsenite (Liao and Yu, 2005; Tseng *et al.*, 2007), although here we report a slightly higher 24 h LC_{50} value of ~5 mM (Supplementary Figure 6). Reduced sensitivity to arsenite is further demonstrated by the fact that only chronic, lifelong exposure to ≥100 μM (~7.5 ppm) arsenite reduce nematode lifespan (~10 to 15%) (Yu *et al.*, 2016), whereas chronic exposure to much lower concentrations (10–150 ppb) of arsenite are associated with increased mortality rates in humans (Argos *et al.*, 2010). Reduced sensitivity is likely, in part, due to the nematode's cuticle, a collagenous barrier that has been shown to limit the absorption of a variety of toxicants, including: bisphenol A (Watanabe *et al.*, 2005), oligomycin (Luz *et al.*, 2015a), and drugs such as nicotine and ivermectin (Partridge *et al.*, 2008). The nematode cuticle is also impermeable to metal ions such as manganese (Au *et al.*, 2009), thus, is likely also impermeable to arsenite. Importantly, the internal dose of arsenite inducing the Warburg effect *in vitro* and *in vivo* is similar, as the amount of arsenite in nematode mitochondria (48 h exposure to 50 μM arsenite) and rat liver cell (RLC16) mitochondria (24 h exposure to 1 μM arsenite) (Naranmandura *et al.*, 2011) is similar (63 vs 5 ng arsenite/mg protein, respectively). Another point to consider is that it takes several weeks of exposure to 1 μM arsenite to induce the Warburg effect *in vitro* (Zhao *et al.*, 2013), whereas a Warburg-like effect was observed in nematodes after 48 h of arsenite exposure.

CONCLUSIONS

Using a combination of novel and established methods including toxicological, biochemical, and genetic techniques, we report that arsenic results in metabolic shifts *in vivo* that are consistent with reported roles of arsenic in carcinogenesis (Zhao *et al.*, 2014), metabolic syndrome (Ditzel *et al.*, 2015; Shi *et al.*, 2013), and other metabolism-related pathologies (Arteel *et al.*, 2008; Sanchez-Soria *et al.*, 2014; Tan *et al.*, 2011). In particular, we report an arsenite-induced Warburg-like effect which has previously only been demonstrated *in vitro*, as well as previously unidentified alterations in mitochondrial respiration (reduced SRC and ATP-linked respiration, and increased proton leak). Finally, we demonstrate that deficiencies in ETC complexes I, II, and III sensitize nematodes to arsenite exposure, thus identifying a novel class of gene–environment interactions that warrant further investigation for their human relevance.

SUPPLEMENTARY DATA

Supplementary data are available online at http://toxsci.oxfordjournals.org/

ACKNOWLEDGEMENTS

We thank Elena Turner and Jonathan Hibshman for their advice and assistance in the extraction of small metabolites for metabolomics analysis.

FUNDING

As a Duke Cancer Institute member, I acknowledge support from the Duke Cancer Institute as part of the P30 Cancer Center Support Grant (Grant ID: P30 CA014236). This work was also supported by the National Institute of Environmental Health Sciences and National Institute of Health (R01-ES017540-01A2 and P42ES010356). The content is solely the responsibility of the authors and does not necessarily represent the official views of the NIH. Several strains were provided by the *C. elegans* Reverse Genetics Core Facility at UBC, which is part of the International *C. elegans* Gene Knockout Consortium and is supported by the National Institute of Health, Office of Research Infrastructure Programs (P40 OD010440). The authors have no conflicts of interest to disclose.

REFERENCES

An, J., Muoio, D. M., Shiota, M., Fujimoto, Y., Cline, G. W., Shulman, G. I., Koves, T. R., Stevens, R., Millington, D., and Newgard, C. B. (2004). Hepatic expression of malonyl-CoA decarboxylase reverses muscle, liver and whole-animal insulin resistance. *Nat. Med.* **10**, 268–274.

Argos, M., Kalra, T., Rathouz, P. J., Chen, Y., Pierce, B., Parvez, F., Islam, T., Ahmed, A., Rakibuz-Zaman, M., and Hasan, R. (2010). Arsenic exposure from drinking water, and all-cause and chronic-disease mortalities in Bangladesh (HEALS): a prospective cohort study. *Lancet* **376**, 252–258.

Arteel, G. E., Guo, L., Schlierf, T., Beier, J. I., Kaiser, J. P., Chen, T. S., Liu, M., Conklin, D. J., Miller, H. L., and von Montfort, C. (2008). Subhepatotoxic exposure to arsenic enhances lipopolysaccharide-induced liver injury in mice. *Toxicol. Appl. Pharmacol.* **226**, 128–139.

Au, C., Benedetto, A., Anderson, J., Labrousse, A., Erikson, K., Ewbank, J. J., and Aschner, M. (2009). SMF-1, SMF-2 and SMF-3 DMT1 orthologues regulate and are regulated differentially by manganese levels in *C. elegans*. *PloS One* **4**, e7792.

Belzacq, A. S., El Hamel, C., Vieira, H., Cohen, I., Haouzi, D., Metivier, D., Marchetti, P., Brenner, C., and Kroemer, G. (2001). Adenine nucleotide translocator mediates the mitochondrial membrane permeabilization induced by lonidamine, arsenite and CD437. *Oncogene* **20**, 7579–7587.

Bergquist, E. R., Fischer, R. J., Sugden, K. D., and Martin, B. D. (2009). Inhibition by methylated organoarsenicals of the respiratory 2-oxo-acid dehydrogenases. *J. Organomet. Chem.* **694**, 973–980.

Bolt, A. M., Douglas, R. M., and Klimecki, W. T. (2010). Arsenite exposure in human lymphoblastoid cell lines induces autophagy and coordinated induction of lysosomal genes. *Toxicol. Lett.* **199**, 153–159.

Boyd, W. A., Smith, M. V., Kissling, G. E., and Freedman, J. H. (2010). Medium-and high-throughput screening of neurotoxicants using *C. elegans*. *Neurotoxicol. Teratol.* **32**, 68–73.

Boyd, W. A., Smith, M. V., Kissling, G. E., Rice, J. R., Snyder, D. W., Portier, C. J., and Freedman, J. H. (2009). Application of a mathematical model to describe the effects of chlorpyrifos on *Caenorhabditis elegans* development. *PLoS One* **4**, e7024.

Braeckman, B. P., Houthoofd, K., and Vanfleteren, J. R. 2009. Intermediary metabolism. WormBook. doi:10.1895/wormbook.1.146.1 ISBN/ISSN: 1551-8507.

Brand, M. D., Affourtit, C., Esteves, T. C., Green, K., Lambert, A. J., Miwa, S., Pakay, J. L., and Parker, N. (2004). Mitochondrial superoxide: production, biological effects, and activation of uncoupling proteins. *Free Radic. Biol. Med.* **37**, 755–767.

Brys, K., Castelein, N., Matthijssens, F., Vanfleteren, J. R., and Braeckman, B. P. (2010). Disruption of insulin signalling preserves bioenergetic competence of mitochondria in ageing *Caenorhabditis elegans*. *BMC Biol.* **8**, 91.

Cline, D. J., Thorpe, C., and Schneider, J. P. (2003). Effects of As (III) binding on α-helical structure. *J. Am. Chem. Soc.* **125**, 2923–2929.

Cooper, A. Jr., and Van Gundy, S. (1971). Ethanol production and utilization by *Aphelenchus avenae* and *Caenorhabditis* sp. *J. Nematol.* **3**, 205.

DiMauro, S., and Schon, E. A. (2003). Mitochondrial respiratory-chain diseases. *N. Engl. J. Med.* **348**, 2656–2668.

Ditzel, E. J., Nguyen, T., Parker, P., and Camenisch, T. D. (2015). Effects of arsenite exposure during fetal development on energy metabolism and susceptibility to diet-induced fatty liver disease in male mice. *Environ. Health Perspect.* 124(2), 201–209.

Falk, M., Zhang, Z., Rosenjack, J., Nissim, I., Daikhin, E., Sedensky, M., Yudkoff, M., and Morgan, P. (2008). Metabolic pathway profiling of mitochondrial respiratory chain mutants in *C. elegans*. *Mol. Genet. Metabol.* **93**, 388–397.

Föll, R. L., Pleyers, A., Lewandovski, G. J., Wermter, C., Hegemann, V., and Paul, R. J. (1999). Anaerobiosis in the nematode *Caenorhabditis elegans*. *Compar. Biochem. Physiol. B: Biochem. Mol. Biol.* **124**, 269–280.

Gilbert-Diamond, D., Li, Z., Perry, A. E., Spencer, S. K., Gandolfi, A. J., and Karagas, M. R. (2013). A population-based case–control study of urinary arsenic species and squamous cell carcinoma in New Hampshire, USA. *Environ. Health Perspect.* **121**, 1154.

HigashiI, T., Maruyama, E., Otani, T., and Sakamoto, Y. (1965). Studies on the isocitrate dehydrogenase. *J. Biochem.* **57**, 793–798.

Hope, I., Arnold, J., McCarroll, D., Jun, G., Krupa, A., and Herbert, R. (1998). Promoter trapping identifies real genes in *C. elegans*. *Mol. Gen. Genet. MGG* **260**, 300–308.

Hosseini, M. J., Shaki, F., Ghazi-Khansari, M., and Pourahmad, J. (2013). Toxicity of arsenic (III) on isolated liver mitochondria: a new mechanistic approach. *Iranian J. Pharm. Res.: IJPR* **12**, 121.

Hughes, M. F. (2002). Arsenic toxicity and potential mechanisms of action. *Toxicol. Lett.* **133**, 1–16.

Jensen, M. V., Joseph, J. W., Ilkayeva, O., Burgess, S., Lu, D., Ronnebaum, S. M., Odegaard, M., Becker, T. C., Sherry, A. D., and Newgard, C. B. (2006). Compensatory responses to pyruvate carboxylase suppression in islet β-cells preservation of glucose-stimulated insulin secretion. *J. Biol. Chem.* **281**, 22342–22351.

Karagas, M. R., Stukel, T. A., and Tosteson, T. D. (2002). Assessment of cancer risk and environmental levels of arsenic in New Hampshire. *Int. J. Hyg. Environ. Health* **205**, 85–94.

Karagas, M. R., Tosteson, T. D., Morris, J. S., Demidenko, E., Mott, L. A., Heaney, J., and Schned, A. (2004). Incidence of transitional cell carcinoma of the bladder and arsenic exposure in New Hampshire. *Cancer Causes Control* **15**, 465–472.

Ke, Q., and Costa, M. (2006). Hypoxia-inducible factor-1 (HIF-1). *Mol. Pharmacol.* **70**, 1469–1480.

Kim, J., Tchernyshyov, I., Semenza, G. L., and Dang, C. V. (2006). HIF-1-mediated expression of pyruvate dehydrogenase kinase: a metabolic switch required for cellular adaptation to hypoxia. *Cell Metabol.* **3**, 177–185.

Kirkpatrick, D., Dale, K., Catania, J., and Gandolfi, A. (2003). Low-level arsenite causes accumulation of ubiquitinated proteins in rabbit renal cortical slices and HEK293 cells. *Toxicol. Appl. Pharmacol.* **186**, 101–109.

Kitchin, K. T., and Wallace, K. (2008). The role of protein binding of trivalent arsenicals in arsenic carcinogenesis and toxicity. *J. Inorg. Biochem.* **102**, 532–539.

Kondo, M., Senoo-Matsuda, N., Yanase, S., Ishii, T., Hartman, P. S., and Ishii, N. (2005). Effect of oxidative stress on translocation of DAF-16 in oxygen-sensitive mutants, mev-1 and gas-1 of *Caenorhabditis elegans*. *Mechanisms Ageing Devel.* **126**, 637–641.

Lagido, C., McLaggan, D., and Glover, L. A. (2015). A screenable in vivo assay for mitochondrial modulators using transgenic bioluminescent *Caenorhabditis elegans*. *JoVE (J. Vis. Exp.)* e53083–e53083.

Lagido, C., Pettitt, J., Flett, A., and Glover, L. A. (2008). Bridging the phenotypic gap: real-time assessment of mitochondrial function and metabolism of the nematode *Caenorhabditis elegans*. *BMC Physiology* **8**, 7.

Lapaille, M., Thiry, M., Perez, E., González-Halphen, D., Remacle, C., and Cardol, P. (2010). Loss of mitochondrial ATP synthase subunit beta (Atp2) alters mitochondrial and chloroplastic function and morphology in Chlamydomonas. *Biochim. Biophys. Acta (BBA)-Bioenergetics* **1797**, 1533–1539.

Lesseur, C., Gilbert-Diamond, D., Andrew, A. S., Ekstrom, R. M., Li, Z., Kelsey, K. T., Marsit, C. J., and Karagas, M. R. (2012). A case–control study of polymorphisms in xenobiotic and arsenic metabolism genes and arsenic-related bladder cancer in New Hampshire. *Toxicol. Lett.* **210**, 100–106.

Lewis, J. A., and Fleming, J. T. (1995). Basic culture methods. *Methods Cell Biol.* **48**, 3–29.

Li, Y. N., Xi, M. M., Guo, Y., Hai, C. X., Yang, W. L., and Qin, X. J. (2014). NADPH oxidase-mitochondria axis-derived ROS mediate arsenite-induced HIF-1α stabilization by inhibiting prolyl hydroxylases activity. *Toxicol. Lett.* **224**, 165–174.

Liao, V. H. C., and Yu, C. W. (2005). *Caenorhabditis elegans* gcs-1 confers resistance to arsenic-induced oxidative stress. *Biometals* **18**, 519–528.

Liaw, J., Marshall, G., Yuan, Y., Ferreccio, C., Steinmaus, C., and Smith, A. H. (2008). Increased childhood liver cancer mortality and arsenic in drinking water in northern Chile. *Cancer Epidemiol. Biomarkers Prevent.* **17**, 1982–1987.

Liu, X., Sadhukhan, S., Sun, S., Wagner, G. R., Hirschey, M. D., Qi, L., Lin, H., and Locasale, J. W. (2015). High resolution metabolomics with acyl-CoA profiling reveals widespread remodeling in response to diet. *Mol. Cell. Proteomics MCP* **M114**, 044859

Luz, A. L., Lagido, C., Hirschey, M. D., and Meyer, J. N. (2016). *In vivo* determination of mitochondrial function using luciferase-expressing *Caenorhabditis elegans*: contribution of oxidative phosphorylation, glycolysis, and fatty acid oxidation to toxicant-induced dysfunction. *Curr. Protoc. Toxicol.* **69**,25.8.1–25.8.22.

Luz, A. L., Rooney, J. P., Kubik, L. L., Gonzalez, C. P., Song, D. H., and Meyer, J. N. (2015a). Mitochondrial Morphology and Fundamental Parameters of the Mitochondrial Respiratory Chain Are Altered in Caenorhabditis elegans Strains Deficient in Mitochondrial Dynamics and Homeostasis Processes. *PloS One* **10**, e0130940.

Luz, A. L., Smith, L. L., Rooney, J. P., and Meyer, J. N. (2015b). Seahorse Xfe24 extracellular flux analyzer-based analysis of

cellular respiration in *Caenorhabditis elegans*. *Curr. Protoc. Toxicol.* **66**, 25.7.1–25.7.15.

Marshall, G., Ferreccio, C., Yuan, Y., Bates, M. N., Steinmaus, C., Selvin, S., Liaw, J., and Smith, A. H. (2007). Fifty-year study of lung and bladder cancer mortality in Chile related to arsenic in drinking water. *J. Natl. Cancer Inst.* **99**, 920–928.

McBride, H. M., Neuspiel, M., and Wasiak, S. (2006). Mitochondria: more than just a powerhouse. *Curr. Biol.* **16**, R551–R560.

Meyer, J. N., Lord, C. A., Yang, X. Y., Turner, E. A., Badireddy, A. R., Marinakos, S. M., Chilkoti, A., Wiesner, M. R., and Auffan, M. (2010). Intracellular uptake and associated toxicity of silver nanoparticles in *Caenorhabditis elegans*. *Aquat. Toxicol.* **100**, 140–150.

Morgan, P., Higdon, R., Kolker, N., Bauman, A., Ilkayeva, O., Newgard, C. B., Kolker, E., Steele, L., and Sedensky, M. (2015). Comparison of proteomic and metabolomic profiles of mutants of the mitochondrial respiratory chain in *Caenorhabditis elegans*. *Mitochondrion* **20**, 95–102.

Myeku, N., and Figueiredo-Pereira, M. E. (2011). Dynamics of the degradation of ubiquitinated proteins by proteasomes and autophagy association With sequestosome 1/p62. *J. Biol. Chem.* **286**, 22426–22440.

Naranmandura, H., Xu, S., Sawata, T., Hao, W. H., Liu, H., Bu, N., Ogra, Y., Lou, Y. J., and Suzuki, N. (2011). Mitochondria are the main target organelle for trivalent monomethylarsonous acid (MMAIII)-induced cytotoxicity. *Chem. Res. Toxicol.* **24**, 1094–1103.

Partridge, F. A., Tearle, A. W., Gravato-Nobre, M. J., Schafer, W. R., and Hodgkin, J. (2008). The *C. elegans* glycosyltransferase BUS-8 has two distinct and essential roles in epidermal morphogenesis. *Devel. Biol.* **317**, 549–559.

Pfeiffer, M., Kayzer, E. B., Yang, X., Abramson, E., Kenaston, M. A., Lago, C. U., Lo, H. H., Sedensky, M. M., Lunceford, A., and Clarke, C. F. (2011). *Caenorhabditis elegans* UCP4 protein controls complex II-mediated oxidative phosphorylation through succinate transport. *J. Biol. Chem.* **286**, 37712–37720.

Rahman, M. (2002). Arsenic and contamination of drinking-water in Bangladesh: a public-health perspective. *J. Health Popul. Nutr.* **3**, 193–197.

Rastogi, S., Borgo, B., Pazdernik, N., Fox, P., Mardis, E. R., Kohara, Y., Havranek, J., and Schedl, T. (2015). *Caenorhabditis elegans* glp-4 encodes a valyl aminoacyl tRNA synthetase. *G3: Genes|Genomes Genet.* **5**, 2719–2728.

Ravenscroft, P., Brammer, H., and Richards, K. (2009). *Arsenic Pollution: A Global Synthesis*, vol. **28**. West Sussex, United Kingdom: John Wiley & Sons.

Robey, R. B., Weisz, J., Kuemmerle, N., Salzberg, A. C., Berg, A., Brown, D. G., Kubik, L., Palorini, R., Al-Mulla, F., and Al-Temaimi, R. (2015). Metabolic reprogramming and dysregulated metabolism: cause, consequence and/or enabler of environmental carcinogenesis? *Carcinogenesis* **36**, S203–S231.

Rooney, J., Luz, A., Gonzalez-Hunt, C., Bodhicharla, R., Ryde, I., Anbalagan, C., and Meyer, J. (2014). Effects of 5′-fluoro-2-deoxyuridine on mitochondrial biology in *Caenorhabditis elegans*. *Exp. Gerontol.* **56**, 69–76.

Rooney, J. P., Ryde, I. T., Sanders, L. H., Howlett, E. H., Colton, M. D., Germ, K. E., Mayer, G. D., Greenamyre, J. T., and Meyer, J. N. (2015). PCR based determination of mitochondrial DNA copy number in multiple species. In Palmeira, Carlos M., Rolo, Anabela P. eds, *Mitochondrial Regulation*, pp. 23–38. Clifton, NJ: Springer.

Sanchez-Soria, P., Broka, D., Quach, S., Hardwick, R. N., Cherrington, N. J., and Camenisch, T. D. (2014). Fetal exposure to arsenic results in hyperglycemia, hypercholesterolemia, and nonalcoholic fatty liver disease in adult mice. *Journal of Toxicology and Health* **1**(1), 1.

Schaefer, A. M., Taylor, R. W., Turnbull, D. M., and Chinnery, P. F. (2004). The epidemiology of mitochondrial disorders—past, present and future. *Biochim. Biophys. Acta (BBA)-Bioenergetics* **1659**, 115–120.

Shi, H., Shi, X., and Liu, K. J. (2004). Oxidative mechanism of arsenic toxicity and carcinogenesis. *Mol. Cell. Biochem.* **255**, 67–78.

Shi, X., Wei, X., Koo, I., Schmidt, R. H., Yin, X., Kim, S. H., Vaughn, A., McClain, C. J., Arteel, G. E., and Zhang, X. (2013). Metabolomic analysis of the effects of chronic arsenic exposure in a mouse model of diet-induced fatty liver disease. *J. Proteome Res.* **13**, 547–554.

Smith, A. H., Marshall, G., Yuan, Y., Ferreccio, C., Liaw, J., von Ehrenstein, O., Steinmaus, C., Bates, M. N., and Selvin, S. (2006). Increased mortality from lung cancer and bronchiectasis in young adults after exposure to arsenic in utero and in early childhood. *Environ. Health Perspect.* 1293–1296.

Stiernagle, T. (1999). Maintenance of *C. elegans*. *C. Elegans* **2**, 51–67.

Tan, M., Schmidt, R. H., Beier, J. I., Watson, W. H., Zhong, H., States, J. C., and Arteel, G. E. (2011). Chronic subhepatotoxic exposure to arsenic enhances hepatic injury caused by high fat diet in mice. *Toxicol. Appl. Pharmacol.* **257**, 356–364.

Thomas, D. J., Li, J., Waters, S. B., Xing, W., Adair, B. M., Drobna, Z., Devesa, V., and Styblo, M. (2007). Arsenic (+3 oxidation state) methyltransferase and the methylation of arsenicals. *Exp. Biol. Med.* **232**, 3–13.

Tsang, W. Y., and Lemire, B. D. (2002). Mitochondrial genome content is regulated during nematode development. *Biochem. Biophys. Res. Commun.* **291**, 8–16.

Tsang, W. Y., and Lemire, B. D. (2003). The role of mitochondria in the life of the nematode, *Caenorhabditis elegans*. *Biochim. Biophys. Acta (BBA)-Mol. Basis Dis.* **1638**, 91–105.

Tsang, W. Y., Sayles, L. C., Grad, L. I., Pilgrim, D. B., and Lemire, B. D. (2001). Mitochondrial Respiratory chain deficiency in *Caenorhabditis elegans* results in developmental arrest and increased life span. *J. Biol. Chem.* **276**, 32240–32246.

Tseng, Y. Y., Yu, C. W., and Liao, V. H. C. (2007). *Caenorhabditis elegans* expresses a functional ArsA. *FEBS J.* **274**, 2566–2572.

Wang, T. S., Hsu, T. Y., Chung, C. H., Wang, A. S., Bau, D. T., and Jan, K. Y. (2001). Arsenite induces oxidative DNA adducts and DNA-protein cross-links in mammalian cells. *Free Radic. Biol. Med.* **31**, 321–330.

Wang, Y., Singh, U., and Mueller, D. M. (2007). Mitochondrial genome integrity mutations uncouple the yeast *Saccharomyces cerevisiae* ATP synthase. *J. Biol. Chem.* **282**, 8228–8236.

Watanabe, M., Mitani, N., Ishii, N., and Miki, K. (2005). A mutation in a cuticle collagen causes hypersensitivity to the endocrine disrupting chemical, bisphenol A, in *Caenorhabditis elegans*. *Mutat. Res. Fund. Mol. Mechanisms Mut.* **570**, 71–80.

Weber, C. I. (1991). *Methods for Measuring the Acute Toxicity of Effluents and Receiving Waters to Freshwater and Marine Organisms*. Cincinnati, Ohio: Environmental Monitoring Systems Laboratory, Office of Research and Development, US Environmental Protection Agency.

Wię, M. R., and Wojtczak, L. (1997). Involvement of the dicarboxylate carrier in the protonophoric action of long-chain fatty

acids in mitochondria. *Biochem. Biophys. Res. Commun.* **232**, 414–417.

Wu, J. Y., Kao, H. J., Li, S. C., Stevens, R., Hillman, S., Millington, D., and Chen, Y. T. (2004). ENU mutagenesis identifies mice with mitochondrial branched-chain aminotransferase deficiency resembling human maple syrup urine disease. *J. Clin. Investig.* **113**, 434.

Yang, W., and Hekimi, S. (2010). Two modes of mitochondrial dysfunction lead independently to lifespan extension in *Caenorhabditis elegans*. *Aging Cell* **9**, 433–447.

Yochem, J., and Greenwald, I. (1989). glp-1 and lin-12, genes implicated in distinct cell-cell interactions in *C. elegans*, encode similar transmembrane proteins. *Cell* **58**, 553–563.

Yu, C. W., How, C. M., and Liao, V. H. C. (2016). Arsenite exposure accelerates aging process regulated by the transcription factor DAF-16/FOXO in *Caenorhabditis elegans*. *Chemosphere*. **150**, 632–638.

Yu, H. S., Liao, W. T., and Chai, C. Y. (2006). Arsenic carcinogenesis in the skin. *J. Biomed. Sci.* **13**, 657–666.

Yuan, Y., Marshall, G., Ferreccio, C., Steinmaus, C., Liaw, J., Bates, M., and Smith, A. H. (2010). Kidney cancer mortality: fifty-year latency patterns related to arsenic exposure. *Epidemiology* **21**, 103–108.

Zhang, T., Qi, Y., Liao, M., Xu, M., Bower, K., Frank, J., Shen, H. M., Luo, J., Shi, X., and Chen, G. (2012). Autophagy is a cell self-protective mechanism against arsenic-induced cell transfomation. *Toxicol. Sci.* **130**(2):298–308.

Zhao, C. Q., Young, M. R., Diwan, B. A., Coogan, T. P., and Waalkes, M. P. (1997). Association of arsenic-induced malignant transformation with DNA hypomethylation and aberrant gene expression. *Proc. Natl. Acad. Sci. USA* **94**, 10907–10912.

Zhao, F., Malm, S. W., Hinchman, A. N., Li, H., Beeks, C. G., and Klimecki, W. T. (2014). Arsenite-induced pseudo-hypoxia results in loss of anchorage-dependent growth in BEAS-2B pulmonary epithelial cells. *PloS One* **9**, e114549.

Zhao, F., Severson, P., Pacheco, S., Futscher, B. W., and Klimecki, W. T. (2013). Arsenic exposure induces the Warburg effect in cultured human cells. *Toxicol. Appl. Pharmacol.* **271**, 72–77.